

SCIENTIFIC REPORTS



OPEN

Optical absorbing origin of chiroptical activity in planar plasmonic metasurfaces

Atefeh Fazel Najafabadi  & Tavakol Pakizeh

As a significant characteristic of many biomolecules, chemical substances, and artificial nanostructures, chirality conduce different types of optical interactions with the spin angular momentum of the impinging light field. Although, chiral arrangement and spatial phase retardation are the key factors for obtaining chirality in three-dimensional (3D) structures, the origin of chirality in the feasible planar structures has not been thoroughly addressed. Here using an intuitive and simple analytical approach, called cross-hybridization model, the essence and properties of the optical chirality of individual planar nanostructures are unveiled. In order to fundamentally address this chirality in terms of circular dichroism (CD), the chiroptical response of a simple dimer composed of the lossy nanoblocks in L-shape arrangement are investigated based on the provided optical interaction and loss effects. The theoretical findings, adequately supported by the numerical calculations, reveal that chiroptical activity occurs predominantly due to handedness-dependent absorption or heating loss in a nanostructured metasurface.

Chiroptical properties of non-superimposable biological molecules and chiral nanostructures on their mirror images, have gained tremendous interest in recent years. Biomolecules mainly show sensitivity to one of the left or right circular polarized light. This results in the investigation the tendency of the biomolecules and construction drugs with an efficient enantiomer¹. Similar to natural materials, well organized artificial metasurfaces indicate different behavior to the spin angular momentum of the light which arises unlike refractive indices and absorption rates for left and right circularly polarized (LCP and RCP, respectively) waves¹⁻⁷. Therefore, novel photonic devices such as circular dichroism metamirrors, optical detectors for Stokes parameters' polarimetry, chiral sensors, and metamaterials for terahertz nonlinear optics and quantum information processing are suggested⁶⁻¹².

However, breaking symmetry in 3D nanostructures is a necessary and sufficient condition for obtaining chirality^{5, 10, 13, 14}, the physical origin of the chirality in planar nanostructures not yet entirely addressed. Recently using a novel developed suit, it has been experimentally shown that CD –the difference in optical properties of LCP and RCP light– in planar metasurfaces occurs due to handedness dependent of ohmic heating¹⁵. Moreover, it has been numerically demonstrated that homogenous structures composed of silicon nanodisks do not posse chirality¹⁶.

Here, the electromagnetic interactions between the simplest planar chiral nanostructure and different spin angular momentum of the incident light are modeled using cross coupled dipoles in quasistatic regime. A dimer of nanoparticles in L-shape arrangement, which might be called meta-atom of an arbitrary metasurface, is considered. This simple building-block conveys interesting and unique optical properties in terms of optical CD, granted by the properly excited and hybridized localized surface plasmon resonances (LSPRs). It is reported that absorption or loss is the major root of chirality in planar metasurfaces composed of optically interacting nanoparticles as their building blocks. Although a planar lossy nanostructure which is non-superimposable on its mirror image show substantially different absorption under the RCP and LCP light illuminations, in a drastic contrast, a lossless one is achiral even its comprising nanoparticles are arranged in a handedness order.

Results and Discussions

In order to theoretically analyze the chiroptical properties of a system composed of nanoparticles, one should first model the nanostructure precisely and derives the optical properties such as absorption (C_{abs}), scattering (C_{sca}), and extinction (C_{ext}) cross-sections. If the size of the nanoparticles is much smaller than the wavelength,

Faculty of Electrical Engineering, K. N. Toosi University of Technology, Tehran, 1631714191, Iran. Correspondence and requests for materials should be addressed to T.P. (email: t.pakizeh@kntu.ac.ir)

modeling each particle with an electric point dipole is satisfactory. This modeling yields the optical properties of the whole structure by solving the coupled-dipole equations (CDE)¹⁷. For an L-shape dimer composed of two nanoparticles with the general properties, the CDE expressed in Eq. (1).

$$P_i - \alpha_i A_{ij} P_j = \alpha_i E_{inc,i} \quad (1)$$

where α_i ($i, j = x, y$) is the electric polarizability of a single nanoparticle^{18,19}, A_{ij} is the cross-coupling term between two nanoparticles, P_j is the amplitude of the induced polarizability vector, and $E_{inc,j}$ is the incident electric field at the location of particle j . It is common to nanosystems that absorption is dominant relative to the scattering, C_{abs} approximates the C_{ext} . However, for planar nanostructures there is not any difference between C_{ext} of the LCP and RCP waves; therefore for determination of the CD_{abs} , the C_{abs} should be calculated with high accuracy²⁰. This aim is achievable by calculation C_{sca} or the power radiated by an array of oscillating dipoles, although negligible. Consequently, the absorption C_{abs} can be written as:

$$C_{abs} = \frac{4\pi k}{|E_{inc}|^2} \sum_{j=x,y} \text{Im}\{P_j \cdot (\alpha_j^{-1})^* P_j^*\} - \frac{2}{3} k^3 \int d\Omega \sum_{j=x,y} [P_j - \hat{n}(\hat{n} \cdot P_j)] \exp(-ik\hat{n} \cdot \mathbf{r}_j)^2 \quad (2)$$

where k is the wave vector, $d\Omega$ is the element of solid angle, \mathbf{r}_j is the vector in the desired direction of scattering, and \hat{n} is the corresponding unit vector²¹. After some rigorous but routine algebra (the details are explained in the Method section), the $CD_{abs} = CD_{abs}^{LCP} - CD_{abs}^{RCP}$ for a chiral system composed of two nanoparticles is reduced to:

$$CD_{abs} = \frac{32\pi}{3} k^4 A_{xy} \frac{|\alpha_x|^2 \text{Im}\{\alpha_y\} - |\alpha_y|^2 \text{Im}\{\alpha_x\}}{|1 - A_{xy}^2 \alpha_x \alpha_y|^2} \quad (3)$$

Using this fundamental and simple relation, we can easily trace the origin of the CD in planar nanostructures. Importantly, since the spatial phase retardation, in the propagation direction is zero for the planar structures, $CD_{ext} = 0$; and as a result and to justify the relation between CD_{abs} , CD_{sca} , and CD_{ext} , $CD_{sca} = -CD_{abs}$ ²². Expectedly, if the nanoparticles are made by setting the denominator of lossless metals or dielectrics, $\text{Im}\{\alpha\} = 0$, so that CD_{abs} vanishes (see Eq. (3)). In this ideal case, the absorption is inherently zero and consequently $CD_{sca} = -CD_{abs} = 0$, and thus no sign of chirality can be seen in the optical properties. Similarly, it has been recently discussed that handedness nanostructure composed of silicon nanodisks breaks to possess chirality; although, they have interpreted this based on non-induced magnetic dipole moments¹⁶. The introduced comprehensive formula in here, i.e. Eq. (3), clearly demonstrates that even if the dipole moments are induced in a lossless nanostructure, it remains achiral. Similarly, it makes that obvious to have CD in the planar nanostructures the optical interaction of the nanoparticles, denoted by A_{xy} , which depends on the arrangement and the separation distance of the nanoparticles, should be noticeable. Importantly, these coupling effects of nanoparticles on each other should differ, depending on the polarization. In the regime where the assumptions of the CDE approach are valid, these could be considered as two crucial criteria for designing chiral nanostructures or meta-atoms for the intended optically active planar metasurfaces.

Additionally, the peaks' positions of the resulting CD_{abs} as well as the elementary absorption, C_{abs} (Eq. 2), of the hybridized LSPR modes, i.e. the in-phase (anti-bonding) and out-of-phase (bonding) modes, are analytically found by setting the denominator in Eq. 3 to zero: $1 - (A_{xy} \alpha)^2 = 0$, by assuming $\alpha_x \approx \alpha_y = \alpha$. Based on this condition, the electric polarizability ($\alpha(\omega) = V(\varepsilon(\omega) - \varepsilon_m)[\varepsilon_m + l(\varepsilon(\omega) - \varepsilon_m)]^{-1}$)²⁰, and the ideal (lossless) Drude model ($\varepsilon(\omega) = \varepsilon_\infty - \omega_p^2/\omega^2$) for the dielectric function of the nanoparticles²³, these energies are found:

$$\omega_\pm^2 = \omega_p^2 / [(\varepsilon_\infty - \varepsilon_m) \pm \varepsilon_m (VA_{xy} \pm l)^{-1}] \quad (4)$$

where ω_p and ε_∞ are the Drude parameters, and V and l are the volume and the static depolarization factor of the nanoparticles or nanoblocks along their major axis.

In the most trivial case, a schematic view of the L-shape dimer composed of two nanospheres with the diameter $2a$ and the interparticle spacing d is illustrated in Fig. 1(a). There, it is acceptable that the vertical finite-sized equivalent dipole in y -direction experiences different surrounding environment (shaded-area A), compared to the nearby horizontal x -dipole (shaded-area B). In this context, since the y -dipole couples more strongly than x -dipole, two separate effective polarizabilities, α_y and α_x , can be considered; where they can be referred to the slightly different effective-sizes of the considered dipoles. Thus, presumably the polarization-dependent optical cross-coupling of these two dipoles leads to the some sort of CD. Figure 1(b) depicts the cross-hybridization model and the induced dipole moments for the L-shape dimer. This can be compared to the conventional hybridization model where the point-dipoles are co-polarized²⁴. Also, the optical extinction efficiency, Q_{ext} of the L-shaped plasmonic nanosystem with $\theta = 25^\circ$, $d = 25$ and $a = 10$ nm, and described by the Drude model with $\omega_p = 8.915$ and $\gamma = 0.477$ eV, which non-uniformly illuminated by the linearly-polarized incident field, $E_{inc,x}$, is depicted in Fig. 1(c) in which the LSPR energy of a single particle (ω_{LSPR}) and the resulting hybridized energies ω_\pm of the considered dimer are determined. Moreover, since the nanoparticles are very close, throughout the paper only the nearfield term in A_{xy} is considered. Thus, based on the arrangement and geometry seen in Fig. 1(a), the term $A_{xy} = -3\sin(2\theta)/(2d^3)$.

In this illustrative case, the relation in Eq. (4) becomes even simpler by assuming the ideal Drude nanospheres with $\varepsilon_\infty = 1$, $l = 1/3$, and $V = a^3/3$, immersed in air ($\varepsilon_m = 1$): $\omega_\pm = \omega_{LSPR} [1 \pm 1/6(a/d)^3 \sin(2\theta)]^{1/2}$; where $\omega_{LSPR} = \omega_p/\sqrt{3}$. Remarkably, it can be also affirmed that cross-coupling term diminishes when the nanoparticles are along the same axis, for instance y -axis or $\theta = 0^\circ$. Nevertheless, degree of freedom for the resonant

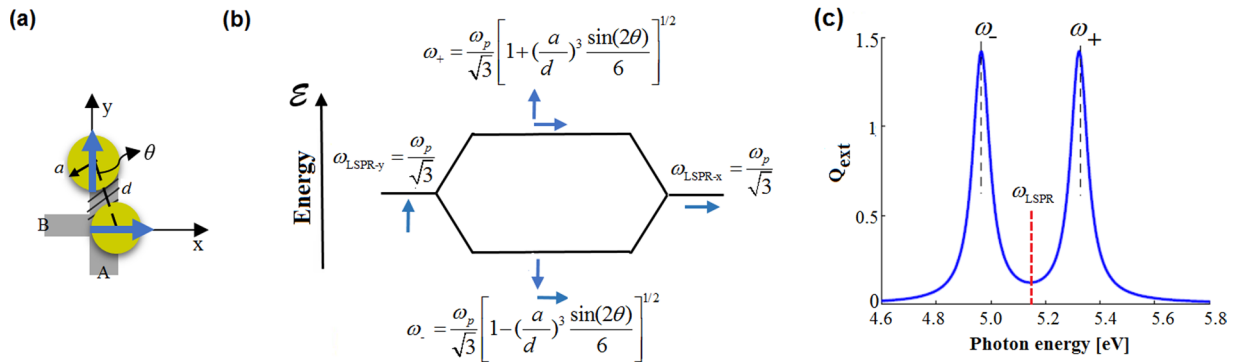


Figure 1. The cross hybridization model and properties. **(a)** Schematic representation of the planar chiral dimer. **(b)** Cross hybridization model of the nanosystem. **(c)** Optical C_{ext} of the Drude dimer presented in **(a)** with $a = 10$ nm, $d = 25$ nm, and $\theta = 25^\circ$. The resonance frequencies of a single particle (ω_{LSPR}) and interacting dimer (ω_{\pm}) are denoted by the dotted vertical lines.

point-dipoles' orientation is infinite in the nanosphere case; and to make this more practical and limited to the chiral case, then one should consider other types of the dipolar LSPRs. Thereby, the nanoblocks, modeled by the prolate nanospheroids, in the same arrangement are employed to reach this goal. It allows only two cross point-dipoles, one on each, to be efficiently excited, in the desired spectral range and upon uniform illuminations. Besides, the optical interaction of these nanoparticles is more pronounced, compared to the nanospheres, which results in substantial polarization-dependent effects. Thus, in the next section, the optical interaction and chiroptical properties of the planar nanostructure composed of nanoblocks are studied in details.

Finding the origin of CD in planar nanostructures, we try to omit complexities and different effective parameters as far as possible. Hence, the nanoparticles are chosen small enough that one can ignore the correction term regarding the energy loss due to radiative reaction¹⁸. Consequently, a dimer of nanoblocks in a handedness arrangement with the length L , same width and height $w = h$, and equal spacing along the x and y axes is selected. The geometry of the dimer is depicted in the inset of Fig. 2(b). In the theoretical modeling, each nanoblock is electromagnetically described by the quasistatic polarizability of a prolate nanospheroid ($a > b = c$), where a , b , and c are the major and minor semiaxis of the spheroid (see inset in Fig. 2(a)). Moreover, the rigorous electromagnetic simulations are performed using the finite integration technique (FIT)²⁵. Several cases are studied to thoroughly investigate the role of different parameters in CD_{abs} . At first the complex dielectric function is described by the Drude model. Then, real metals with the experimentally tabulated permittivities, as more practical and sensible cases, are studied.

CD of the Drude planar nanostructures. In the section, we employ a dimer of Drude nanoblocks with $L = 80$ nm, $w = h = 20$ nm, and equal gap spacing along the x - and y -axes, $g = 10$ nm. Accordingly, in the modeling, the nanospheroids with $2b = 2c = 17$ nm, and $d = 50$ nm are considered (see insets in Fig. 2(a,b)). However, for the x -oriented nanospheroid $2a = 80$ nm and the for other one 82 nm, effectively accounting for stronger interaction about the finite-sized gap area and along y -axis, as previously discussed in terms of α_x and α_y . The LCP and RCP plane-waves are illuminated to the structure from the top. To easily address the roles of the parameters like crucial absorption in the observed phenomenon, the complex dielectric function is described by the Drude model in which the parameters ε_{∞} , ω_p , and γ in order are 9.068, 8.915, and 0.477 eV, partially fitted to the experimental data of gold²³. Nevertheless, the general trend of CD_{abs} in terms of different losses remains ambiguous. The normalized imaginary-part of α of a nanospheroid, based on physical parameters is given by:

$$\text{Im}\{\alpha\} = \frac{\varepsilon'' \varepsilon_m}{[(l\varepsilon' + (1-l)\varepsilon_m)^2 + l^2\varepsilon''^2]} \quad (5)$$

where $\varepsilon = \varepsilon' + i\varepsilon''$ is the complex dielectric constants of the nanoparticle. It is obvious that behaves non-linearly in terms of $\text{Im}\{\varepsilon\} = \varepsilon''$, which is responsible for optical loss, and this indicates that the relation between CD_{abs} and the loss needs a closer look. Figure 2(a) presents theoretical results of $\text{Max}\{CD\}$ versus γ , generally confirmed by the results of the numerical computation shown in Fig. 2(b). In this figure, columns (c) and (d) show the CD_{abs} by considering different γ that are determined on the curves in Fig. 2(a,b) by red and blue points. In this regard, the points A/A' refer to the more realistic value of γ for gold²³. It can be seen that by reducing the value of γ (corresponding to loss), the CD increases at first, and then sharply decreases. Physically, according to Eq. 3, the both terms $\text{Im}\{\alpha\}$ and $|\alpha|^2$ determine CD_{abs} . Although, in the extreme case of $\gamma = 0$, $\varepsilon'' = 0$, and ultimately $\text{Im}\{\alpha\}$ and thereby CD_{abs} diminishes. One should also consider that, by decreasing γ , the intensity of the point dipole oscillator ($|\alpha|^2$) increases and for some values, compensates the reduction of $\text{Im}\{\alpha\}$ in the amplitude of CD_{abs} (Eq. 3). However, by further reduction of γ , it declines and has a dominant role in the amplitude of CD_{abs} . It is valuable to note that by decreasing γ , the CD_{abs} exhibits a narrower spectral line-shape. A comparison between the results of the modeling and the simulated ones confirms that the general trends are qualitatively supported by the CDE model. Indeed, the black dashed-lines in Fig. 2(c1) show $\lambda_{\text{CD}\pm}$ that are calculated using the Eq. (4). Based on this

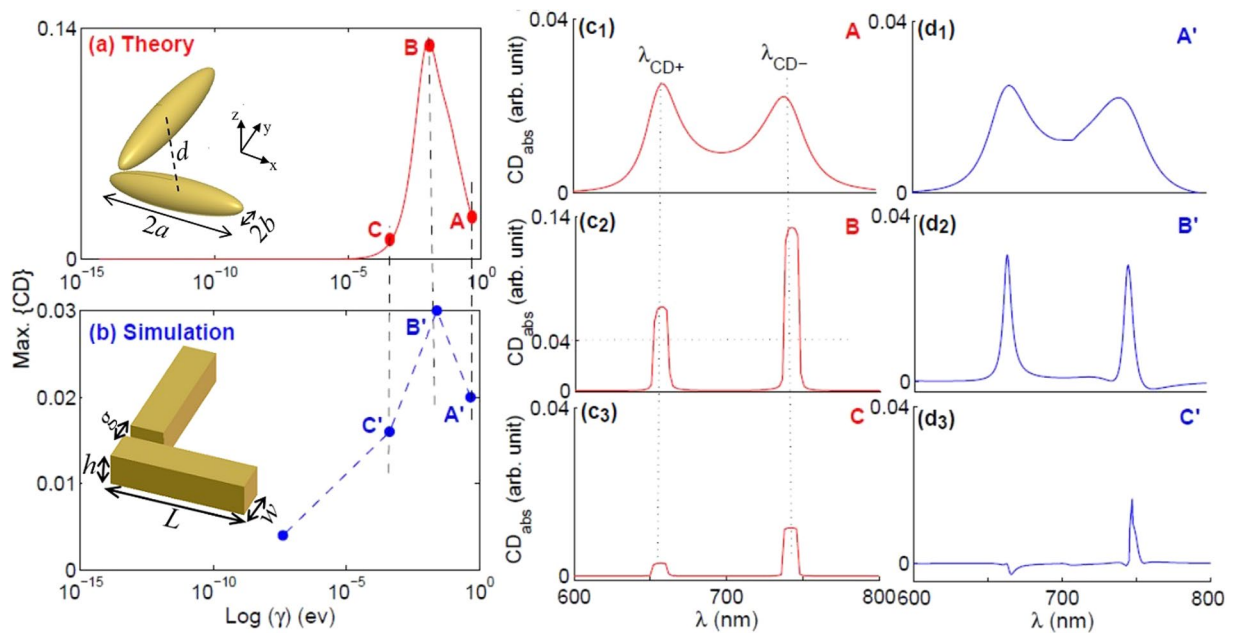


Figure 2. The CD_{abs} trend versus damping-factor γ in a dimer of Drude nanoblocks. Max. $\{CD_{abs}\}$ in terms of γ , theoretically (a) and numerically (b), are shown. The column (c) shows the theoretical CD_{abs} spectra for three specified values of γ , red points at Fig. 1(a). Corresponding numerical results are depicted in the right-column (d). The geometric parameters are $2a = 80$ nm, $2b = 17$ nm, $d = 50$ nm, $L = 80$ nm, $w = h = 20$ nm, and $g = 10$ nm. The vertical black dashed-lines in the c-column denote the fix $\lambda_{CD\pm}$ of the Au dimer.

equation, the optical properties of the Au, and the dimensions of the nanoblocks the resonant wavelengths of the cross hybridized modes are $\lambda_{CD-} = 653$ nm and $\lambda_{CD+} = 740$ nm.

CD of the planar Au-, Ag-, and Ni-nanostructures. In order to proceed and complete the discussions, we also study CD of the plasmonic dimer composed of well-known metals with different absorption such as silver (Ag), gold (Au), and nickel (Ni), in according with ‘best-good-bad’ manner. The dielectric constants of the metals, adopted from the tabulated data in refs 26 and 27. For the assumed three pragmatic cases, the length (L) of the nanoparticles is defined in such a way that the LSPR, in the case of a single nanoblock, occurs nearly at the same wavelength or energy. Therefore, Au-, Ag-, and Ni-nanoparticles with lengths $L = 80$ nm, 100 nm, and 130 nm are adopted, respectively. The resonances of single ones are $\sim \lambda = 700$ nm. Figure 3(a) indicates the real and imaginary parts of the dielectric functions of the considered metals. Figure 3(b) and (c) show the $\text{Im}\{\alpha\}$ and $|\alpha|$, the two major terms of Eq. (3), for the induced dipole in the nanospheroids along the major axis, respectively. As mentioned before, the nanoblocks are modeled with prolate nanospheroids with slightly different $2a$, which are schematically depicted in Fig. 3(b). As seen in the Fig. 3(a); although, Ni has more losses, in comparison with two other metals, and Ag has the least loss, in contrast $\text{Im}\{\alpha\}$ and $|\alpha|$ of the Ag-nanoparticle is substantial. This result marks at this point that smaller value of ϵ'' , does not always mean smaller $\text{Im}\{\alpha\}$ and $|\alpha|$. Based on the indirect relation explained in Eq. 5, in these cases reduction of the Im-part of optical constant, i.e. ϵ'' , not only increases the intensity of the corresponding resonant dipole but also raises the Im-part of the resulting polarizability. Figure 3(d,e, and f) indicate the both theoretical and numerical CD for dimers made of different metals. As expected from the results of Fig. 3(b) and (c), the induced optical CD of the dimer composed of Ni is less than others; and interestingly the Ag-dimer demonstrates the highest CD among the considered cases, unrespecting to its volume. The second and third rows of Fig. 3 show the theoretical and numerical results, respectively. It can be seen there is a remarkably close correspondence between those results. It should be also noted that since the dimensions of these three dimers are not the same, A_{xy} may be slightly different; although, these variations are minor compared to the major effects raised from the polarizabilities, α_x and α_y , removing any ambiguity. Based on these results, it can be stressed there is indirect relation between the amounts of loss (ϵ'') and the CD intensities of single dimers made of lossy Ni, Au, and Ag. The later displays stronger CD, owing to the roles of optical properties of the single low-loss Ag-nanoparticles and their strong optical interactions in the dimer configuration.

To further address the difference between the optical properties of the LCP and RCP illuminations upon the considered planar plasmonic nanostructure, the power loss densities (P_{Loss}) are shown at the peaks’ positions of the observed CD_{abs} spectra or the cross-hybridized LSPRs for a dimer of Au nanoblocks (Fig. 3-e₂). According to the theory of the hybridized modes, bonding and anti-bonding, are induced in the system at $\lambda = 665$ and 742 nm, respectively. The power absorptions and scattering are different for the LCP and RCP incident waves. The power loss densities are shown in Fig. 4 when the structure is illuminated with RCP (a_1, b_1) and LCP (a_2, b_2) plane-waves. Interestingly, the power loss is higher at the nanoblock along the y-axis when the RCP excites the dimer; although, as seen in Figs 4(a_2 and b_2) it is reversed for the case of the LCP. The difference between

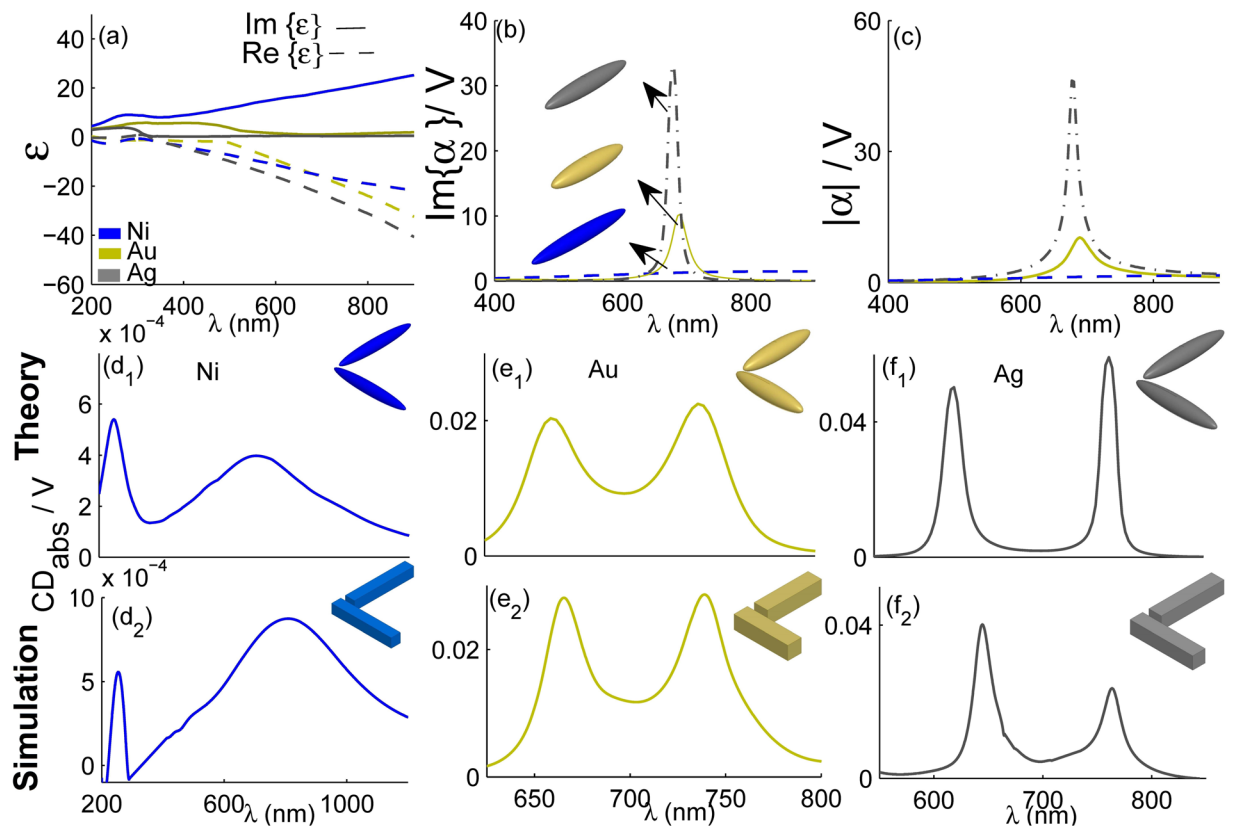


Figure 3. Optical properties of Au, Ag, and Ni nanoparticles. The dielectric function of the metals, normalized $\text{Im}\{\alpha\}$ and $|\alpha|$ of the nanospheroids, corresponding to nanoblocks with $L = 80$ nm, 100 nm, and 130 nm composed of Au, Ag, and Ni, are shown in the first-row (**a,b,c**). The theoretical results for CD_{abs} of the dimers composed of these metals shown in the second-row are compared with the corresponding numerical results in the third-row.

power loss densities (ΔP_{Loss}) of the LCP and RCP incident waves for the hybridized modes are plotted in the right-column of Fig. 4. However the optical loss profiles computed for Ag dimer are very similar in trends (not shown) but with higher strengths (see Fig. 3f), the polarization-dependent loss distributions P_{Loss} and ΔP_{Loss} are plotted for Au nanoblocks, relying on gold's practical considerations such as fabrication, engineering, and compatibility issues. Finally, the introduced effects and extended results provide a basic physical description of the CD phenomena in the feasible planar nanostructures which has a remarkable importance in the field of chiral spectroscopy, nanooptics, and nanophotonics.

Conclusion

The origin of optical activity in planar metallic nanostructures was physically discussed. Based on the developed theory and the cross-hybridization model which led to the neat expressions in the quasistatic regime, it was reported that handedness dependent optical interactions influencing the absorptions are crucial and necessary for the observed optical CD in these plasmonic nanostructures. The convenient Drude model was employed to justify the theoretical predictions, and mainly to elaborate on how the loss influences the observed phenomenon. In this regard, it is straightforwardly concluded that any lossless planar dielectric or metallic structure fails to exhibit any CD, even though, they are arranged in a handedness setting with or without strongly optical interacting parts. By considering Ni, Au, and Ag as more practical cases, it was illustrated that later material exhibit stronger CD_{abs} , compromising the loss effect. The presented results deepen the physical understanding and they may prompt new viable designs and related applications in the advanced and sound opto-chiral areas.

Methods

For theoretical analysis, the nanoblocks are modeled by the prolate nanospheroids and the electric polarizabilities are calculated using the semi-analytical formula for the polarizability of prolate²⁸:

$$\alpha(\omega) = \frac{V}{4\pi} \frac{(\epsilon - \epsilon_m)}{\epsilon_m + \left(L_x - i \frac{k^3 V}{6\pi} - \frac{k^2 V}{4\pi} D_x \right) (\epsilon - \epsilon_m)} \quad (6)$$

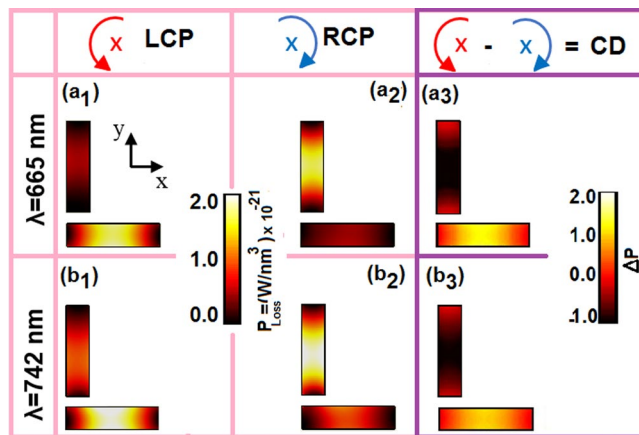


Figure 4. Power loss densities in the Au nanoblocks at the in-phase ($\lambda = 665$ nm) and out-of-phase (742 nm) hybridized LSPR modes for the RCP (a_1, b_1) and LCP (a_2, b_2) cases, respectively. The associated differences in the power loss densities (CD) are shown in (a_3, b_3).

which $V = 4\pi abc/3$ is the particle volume. ε and ε_m are the dielectric coefficients of the nanoparticle and the surrounding medium, respectively. The parameters L_x and D_x are the static and dynamic depolarization factors of the prolate along the x-axis. Using the CDE (Eq. 1), the modified polarizabilities are obtained as:

$$P_i = \frac{E_{inc,i} + A_{12}\alpha_i E_{inc,j}}{1 - (\alpha_i A_{12})^2} \quad i, j = x, y \quad (7)$$

substitution Eq. (7) into Eq. (2) for LCP and RCP incident fields individually, considering $d\Omega = \sin^2(\theta)d\theta d\phi$, $\exp(-ik\hat{n}\cdot\mathbf{r}_i) \approx 1 - ik\hat{n}\cdot\mathbf{r}_i$, and obtaining Eq. (2) on the entire space $0 < \theta < \pi$, ($0 < \varphi < 2\pi$), C_{abs} is calculated. The difference between C_{abs} for LCP and RCP light result in Eq. (3). In the simulation procedure, we use the Finite Integration Technique (FIT). The results are obtained for isolated dimers in the simulation volume which is set to the $\lambda_0/4$ (a quarter of the resonant wavelength of a single nanorod). Tetrahedral meshes with cell size within 1–6 nm are applied in the dimer region. The perfectly matched layer (PML) boundary condition with the reflection level < 0.0001 is used to model the free space.

References

- Boriskina, S. & Zheludev, N. I. *Singular and Chiral Nanoplasmonics* (CRC Press (2014)).
- Tian, X., Fang, Y. & Sun, M. Formation of enhanced uniform chiral fields in symmetric dimer nanostructures. *Sci. Rep.* **5**, 17534 (2015).
- Wang, Z. *et al.* Enhancing circular dichroism by super chiral hot spots from a chiral metasurface with apexes. *Appl. Phys. Lett.* **110**, 221108, doi:10.1063/1.4984920 (2017).
- Zhao, Y., Belkin, M. A. & Alù, A. Twisted optical metamaterials for planarized ultrathin broadband circular polarizers. *Nat. Commun.* **3**, 870, doi:10.1038/ncomms1877 (2012).
- Chen, K. *et al.* Dynamic control of asymmetric electromagnetic wave transmission by active chiral metamaterial. *Sci. Rep.* **7**, 42802, doi:10.1038/srep42802 (2017).
- Wang, Z. *et al.* Circular dichroism metamirrors with near-perfect extinction. *ACS Photonics* **3**, 2096–2101, doi:10.1021/acsp Photonics.6b00533 (2016).
- Friese, D. H. & Ruud, K. Three-photon circular dichroism: towards a generalization of chiroptical non-linear light absorption. *Phys. Chem. Chem. Phys.* **18**, 4174–4184 (2016).
- Wu, C. *et al.* Fano-resonant asymmetric metamaterials for ultrasensitive spectroscopy and identification of molecular monolayers. *Nat. Mater.* **11**, 69–75, doi:10.1038/nmat3161 (2012).
- Hooper, D. C. *et al.* Strong rotational anisotropies affect nonlinear chiral metamaterials. *Adv. Mater.* **29**, 1605110, doi:10.1002/adma.201605110 (2017).
- Tang, Y. & Cohen, A. E. Enhanced enantioselectivity in excitation of chiral molecules by superchiral light. *Science* **332**, 333–336 (2011).
- Li, G., Zhang, S. & Zentgraf, T. Nonlinear photonic metasurfaces. *Nat. Rev. Mater.* **2**, 17010, doi:10.1038/natrevmats.2017.10 (2017).
- Zhao, Y. *et al.* Chirality detection of enantiomers using twisted optical metamaterials. *Nat. Commun.* **8**, 14180, doi:10.1038/ncomms14180 (2017).
- Yin, X. *et al.* Active chiral plasmonics. *Nano Lett.* **15**, 4255–4260, doi:10.1021/nl5042325 (2015).
- Govorov, A. O. Chiral nanoparticle assemblies: circular dichroism, plasmonic interactions, and exciton effects. *J. Mat. Chem.* **21**, 16806–16818 (2011).
- Khanikaev, A. *et al.* Experimental demonstration of the microscopic origin of circular dichroism in two-dimensional metamaterials. *Nat. Commun.* **7**, 12045, doi:10.1038/ncomms12045 (2016).
- Banzer, P., Woźniak, P., Mick, U., De Leon, I. & Boyd, R. W. Chiral optical response of planar and symmetric nanotrimers enabled by heteromaterial selection. *Nat. Commun.* **7**, 13117, doi:10.1038/ncomms13117 (2016).
- Alavi Lavasani, S. H. & Pakizeh, T. Color-switched directional ultracompact optical nanoantennas. *J. Opt. Soc. Am. B* **29**, 1361–1366 (2012).
- Pakizeh, T., Abrishamian, M. S., Granpayeh, N., Dmitriev, A. & Käll, M. Magnetic-field enhancement in gold nanosandwiches. *Opt. Express* **14**, 8240–8246 (2006).
- Kelly, K. L., Coronado, E., Zhao, L. L. & Schatz, G. C. The optical properties of metal nanoparticles: the influence of size, shape, and dielectric environment. *J. Phys. Chem. B* **107**, 668–677, doi:10.1021/jp026731y (2003).
- Najafabadi, A. F. & Pakizeh, T. Analytical chiroptics of the 2D and 3D nanoantennas. *ACS photonics* **4**, 1447–1452 (2017).

21. Draine, B. T. The discrete-dipole approximation and its application to interstellar graphite grains. *Astrophys. J.* **333**, 848–872 (1988).
22. Ogier, R., Fang, Y., Svedendahl, M., Johansson, P. & Käll, M. Macroscopic layers of chiral plasmonic nanoparticle oligomers from colloidal lithography. *ACS Photonics* **1**, 1074–1081 (2014).
23. Vial, A., Grimault, A. S., Macías, D. & Barchiesi, D. & de La Chapelle, M. L. Improved analytical fit of gold dispersion: Application to the modeling of extinction spectra with a finite-difference time-domain method. *Phys. Rev. B* **71**, 085416(7) (2005).
24. Prodan, E., Radloff, C., Halas, N. J. & Nordlander, P. A hybridization model for the plasmon response of complex nanostructures. *Science* **302**, 419–422 (2003).
25. Weiland, T. Finite Integration Method and Discrete Electromagnetism In *Computational Electromagnetics* (ed. Carstensen, C., Funken, S., Hackbusch, W., Hoppe, R. W. & Monk, P.) 183–198 (Springer-Verlag Berlin Heidelberg, 2003).
26. Johnson, P. B. & Christy, R. W. Optical constants of the noble metals. *Phys. Rev. B* **6**, 4370–4379 (1972).
27. Johnson, P. B. & Christy, R. W. Optical constants of transition metals: Ti, v, cr, mn, fe, co, ni. *Phys. Rev. B* **9**, 5056–5070 (1974).
28. Najafabadi, A. F. & Pakizeh, T. Optical properties of plasmonic nanopillars in extended quasi-static limits. *J. Opt. Soc. Am. B* **33**, 511–518 (2016).

Author Contributions

T.P. conceived the basic idea. A.F. performed the analytical modeling and simulations. A.F. and T.P. contributed to the conception, designs, and analyzing the data. Both authors contributed to the scientific discussions and writing of the manuscript. T.P. supervised the research and associated developments.

Additional Information

Competing Interests: The authors declare that they have no competing interests.

Publisher's note: Springer Nature remains neutral with regard to jurisdictional claims in published maps and institutional affiliations.



Open Access This article is licensed under a Creative Commons Attribution 4.0 International License, which permits use, sharing, adaptation, distribution and reproduction in any medium or format, as long as you give appropriate credit to the original author(s) and the source, provide a link to the Creative Commons license, and indicate if changes were made. The images or other third party material in this article are included in the article's Creative Commons license, unless indicated otherwise in a credit line to the material. If material is not included in the article's Creative Commons license and your intended use is not permitted by statutory regulation or exceeds the permitted use, you will need to obtain permission directly from the copyright holder. To view a copy of this license, visit <http://creativecommons.org/licenses/by/4.0/>.

© The Author(s) 2017